Archive of Applied Mechanics (2021) 91:859–881
https://doi.org/10.1007/s00419-020-01793-1

ORIGINAL

Fatima Zohra Zaoui · Djamel Ouinas · Abdelouahed Tounsi · Jaime Aurelio Viña Olay · Belkacem Achour · Mabrouk Touahmia

Fundamental frequency analysis of functionally graded plates with temperature-dependent properties based on improved exponential-trigonometric two-dimensional higher shear deformation theory

Received: 1 April 2020 / Accepted: 17 September 2020 / Published online: 8 October 2020

Abstract The objective of this paper is to provide a computational method to analyze free vibrations of advanced composite plates in thermal environments according to a recently developed higher-order shear deformation theory. This method is based upon the assumptions that displacements field include just four unknowns and considers a combination of trigonometric and exponential shear shape functions which satisfy shear stress free boundary conditions on the plate surfaces. The FG plates are simply supported and subjected to uniform, linear, nonlinear and sinusoidal temperature rise. The temperature field considered is assumed to vary in the thickness direction and constant in the axial directions of plates. It is supposed that the constituent materials possess temperature-dependent properties changing across the thickness with a simple power law function. The equations of motion are obtained by employing Hamilton's principle and solved based on Navier's method to determine natural frequencies of the FG plate. A parametric study for FGM plates with different values of power law index and under different sets of thermal environmental conditions has been carried out. The obtained results are compared for temperature-dependent and temperature-independent FG Plates and validated with available results in the literature.

Keywords Vibration · Functionally graded plate · Shear deformation theory · Temperature-dependent properties · Hamilton's principle

F. Z. Zaoui (✉) · D. Ouinas
Laboratory of numerical and experimental modelling of the mechanical phenomena, Mechanical Engineering Department, Faculty of Sciences and Technology, Ibn Badis University, 27000 Mostaganem, Algeria
E-mail: tima22000@hotmail.com; fatima.zaoui@univ-mosta.dz

A. Tounsi
Material and Hydrology Laboratory, Civil Engineering Department, Faculty of Technology, Sidi Bel Abbes University, 22000 Sidi Bel Abbés, Algeria

A. Tounsi
Department of Civil and Environmental Engineering, King Fahd University of Petroleum and Minerals, Dhahran, Eastern Province 31261, Kingdom of Saudi Arabia

J. A. Viña Olay
Department of Materials Science and Metallurgical Engineering, University of Oviedo, Gijón, Spain

B. Achour · M. Touahmia
Civil Engineering Department, University of Ha'il, Ha'il, Kingdom of Saudi Arabia

1 Introduction

Functionally graded materials (FGMs) are a new family of advanced composites. They are fabricated from the combination of ceramics that provides a high temperature resistance due to its low thermal conductivity and metals which possess good fracture toughness [1]. FGMs are characterized by a smooth and continuous variation of mechanical properties along their thickness to avoid material discontinuity and interface problems, diminishing therefore thermal stress concentrations and deflections [2]. Nowadays, these new materials are widely used as structural components exposed to higher temperature fields such as thermal barrier coatings for ceramic engines, gas turbines, nuclear fusions, optical thin layers, biomaterial electronics, etc. [3–10]. Thus, it is important to develop analysis methods to study the behavior and the response of FGMs under different mechanical loading and environmental conditions.

The literature review reveals that many researchers developed different theories to study the thermo-mechanical [11–14] and dynamic [15–19] behaviors of functionally graded structural components. Based on Reddy's higher-order shear deformation plate theory, Shen [20] analyzed nonlinear bending of a simply supported functionally graded rectangular plate under a sinusoidal or transverse uniform load in thermal environments. This study was extended by Yang and Shen [21] to provide analytical solutions for nonlinear free and forced vibration of FGM plates in thermal environments with different boundary conditions. Huang et al. [22] studied the nonlinear vibration and dynamic response of temperature dependent FG plates in thermal environment based on the higher-order shear deformation theory. Vibration characteristics of pre-stressed temperature-dependent FG rectangular plates were studied by Kim [23] using the Rayleigh–Ritz method based on the third-order shear deformation theory. Chen et al. [24] derived nonlinear partial differential equations for the vibration motion of an initially stressed temperature-independent FGP. By using a quasi-3D HSDT, Zenkour and Alghamdi [25] analyzed the response of FG sandwich plates subjected to thermal load. Li et al. [26] studied the free vibration of functionally graded material beams with surface-bonded piezoelectric layers in thermal environment. Shariyat [27,28] analyzed the linear and nonlinear bending response of sandwich plate under thermo-mechanical loads based on generalized 3D high-order double superposition global–local theory, respectively. Free vibration analysis of symmetric FGM beams subjected to initial thermal stresses was performed by Mahi et al. [29]. Shahrjerdi et al. [30] investigated the temperature-dependent free vibration of solar functionally graded plates subjected to uniform, linear, nonlinear, heat-flux and sinusoidal temperature fields were investigated by using a second-order shear deformation theory (SSDT). Kiani and Eslami [31] studied the buckling and Post-buckling behaviors of imperfect temperature-dependent sandwich plates with functionally graded material (FGM) face sheets on elastic foundation under uniform temperature rise loading. Based on the FSDT, the dynamic behavior of FG Plates in thermal environment supposed to a moving load and elastic foundation was studied by Malekzadeh and Monajjemzadeh [32] by including the effects of initial thermal stresses. Zhang [33] studied the nonlinear bending of FGM rectangular plates with various supported boundaries resting on two-parameter elastic foundations under thermal effect by using physical neutral surface and high-order shear deformation theory. Thermal vibrations of a reinforced orthotropic beams with fibers functionally oriented and graded along the thickness direction are analyzed by Nejati et al. [34] in which uniform thermal distribution was applied throughout the beam and property of the fiber functionally graded beam considered temperature-dependent. The Hierarchical Trigonometric Ritz Formulation (HTRF) had been applied by Fazzolari [35] to study free vibration and thermal stability of FG sandwich plates. The free vibration responses of temperature dependent FG curved panels under thermal environment were analyzed by Kar and Panda [36]. Attia et al. [37] presented four variable higher-order shear deformation theories to analyze free vibration of temperature dependent FG plates. Ibrahimi and Barati [38] presented a theoretical study for thermo-mechanical buckling of size-dependent magneto-electro-thermo-elastic functionally graded (METE-FG) nanoplates in thermal environments based on a refined trigonometric plate theory. The effect of porosities on the vibration of functionally graded rectangular plates subjected to different temperature fields had been studied by Wang and Zu [39]. A novel hyperbolic shear deformation theory for free vibration analysis of simply supported functionally graded plates in thermal environment was developed by Taleb et al. [40]. Shahsavari et al. [41] developed a novel quasi-3D hyperbolic theory to investigate the free vibration of FG plates with porosities resting on Winkler/Pasternak/Kerr foundation. Thang et al. [42] studied the elastic buckling and free vibration of porous-cellular plates with uniform and non-uniform porosity distributions. Based on higher-order shear deformation theory with eight-unknowns, Tu et al. [43] analyzed the vibration of functionally graded plates in thermal environments.

As seen from the above literature review, researchers are getting a real interest in investigating the free vibration of FG structures in thermal environment; this is due to the widespread use of engineering structures

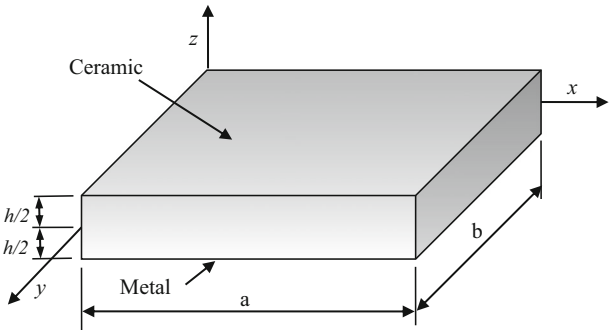

Fig. 1 Schematic representation of rectangular FG plate

including FGM in high temperature environments. Thus, the aim of this work is to extend a recently developed shear deformation theory by Zaoui et al. [44] for providing a computational model for free vibration of functionally graded plates in thermal environments. The displacement fields of the proposed theory include undetermined integral terms and contain fewer unknowns. The novelty of this theory is the use of a new shear strain shape function which is a combination of exponential and trigonometric shear deformation shape functions that considers an adequate distribution of the transverse shear strains across the plate thickness and tangential stress-free boundary conditions on the plate boundary surface without introducing a shear correction factor. The FG plates are considered simply supported and subjected at the upper and lower surfaces to uniform, linear, nonlinear and sinusoidal thermal conditions. Mechanical properties are assumed to be temperature-dependent and varying through the thickness according to a simple power law distribution. The energy method is used to determine the equations of motion which are solved based on Fourier series that satisfy the boundary conditions. The obtained results are validated by comparing them with the results of other studies. The influence of material compositions, plate geometry and temperature fields on the natural frequencies of FG plates are analyzed.

2 Computational modeling

2.1 Material properties

In this work, a rectangular plate with uniform thickness h, length a and width b, made of FGM (Fig. 1), is considered. The rectangular Cartesian coordinate system x, y, z has the surface $z = 0$, coinciding with the mid-plane of the plate. The material properties are taken to be temperature-dependent and vary continuously through the thickness according to the following power law variation expression [23,30]

$$\Gamma(z, T) = (P_c(T) - P_m(T)) \cdot V_c(z) + P_m(T) \tag{1a}$$

$$V_c(z) = \left(\frac{z}{h} + \frac{1}{2}\right)^p \tag{1b}$$

where Γ represents the effective material property such as Young's modulus E, the Poisso's ratio ν, mass density ρ and the thermal expansion coefficientsα of FG plates. P_c and P_m are the temperature-dependent properties of ceramic and metal, respectively. V_c is the volume fraction of the ceramic constituent of the FGM and p is the power-law index that indicates the material variation profile within the thickness [45]. As assumed, the constituent materials possess temperature-dependent properties which can be expressed as a function of temperature [45–47]

$$P(T) = P_0\left(P_{-1}T^{-1} + 1 + P_1T + P_2T^2 + P_3T^3\right) \tag{2}$$

where P indicates material property and T signifies the environment temperature. P_{-1}, P_0, P_1, P_2 and P_3 are coefficients of temperature in Kelvin and are unique to each constituent. Specific values of these constituents of some FGP material components used in this study are presented in Table 1 [47]. The Poisson ratio ν and thermal conductivity k are assumed to be temperature independent due to their small variation with temperature.

Table 1 Temperature-dependent coefficients for ZrO_2/Ti−6Al−4V and SI_3N_4/SUS304 [47]

Materials	P_{-1}	P_0	P_1	P_2	P_3
E					
SUS304	0	201.04e+9	3.079e-3	− 6.534e-7	0
SI_3N_4	0	348.43e+9	− 3.070e-4	2.160e-7	− 8.946e-11
Ti–6Al–4V	0	122.56e+9	− 4.586e-4	0	0
ZrO_2	0	244.27e+9	− 1.371e-3	1.214e-6	− 3.681e-10
ν					
SUS304	0	0.3262	− 2.002e-4	3.797e-7	0
SI_3N_4	0	0.2400	0	0	0
Ti–6Al–4V	0	0.2888	1.108e-4	0	0
ZrO_2	0	0.3330	0	0	0
ρ					
SUS304	0	8166	0	0	0
SI_3N_4	0	2370	0	0	0
Ti–6Al–4V	0	4429	0	0	0
ZrO_2	0	3000	0	0	0
α					
SUS304	0	12.330e-6	8.086e-6	0	0
SI_3N_4	0	5.8723e-6	9.095e-6	0	0
Ti–6Al–4V	0	7.5788e-6	6.638e-4	− 3.147e-6	0
ZrO_2	0	12.766e-6	− 1.491e-3	1.006e-5	− 6.778e-11
k					
SUS304	0	12.04	0	0	0
SI_3N_4	0	9.19	0	0	0
Ti–6Al–4V	0	7.82	0	0	0
ZrO_2	0	1.80	0	0	0

2.2 Temperature field

In this work, four cases of one-dimensional temperature variation according to the thickness are considered, with $T = T(z)$

2.2.1 Uniform temperature

In this case, a uniform temperature field is utilized as given below

$$T(z) = T_0 + \Delta T(z) \tag{3}$$

where $T(z)$ indicates the temperature change, $\Delta T(z)$ is the temperature rise only through the thickness direction and $T_0 = 300(K)$ is room temperature.

2.2.2 Linear temperature

Supposing temperatures T_b and T_t are imposed at the bottom and top of the plate, the temperature field under linear temperature rise through the thickness can be expressed as

$$T(z) = T_0 + T_b + \Delta T\left(\frac{z}{h} + \frac{1}{2}\right) \tag{4}$$

where $\Delta T = T_t - T_b$ specifies the temperature gradient and $T_0 = 300(K)$ is room temperature

2.2.3 Nonlinear temperature

The influence of nonlinear temperature rise is considered across the plate's thickness. This field of temperature is defined by solving the one dimensional steady-state heat conduction equation given in Eq. (5).

$$-\frac{\mathrm{d}}{\mathrm{d}z}\left(k(z)\frac{\mathrm{d}T}{\mathrm{d}z}\right) = 0 \tag{5}$$

with the boundary conditions $T\,(h/2) = T_0 + T_t$ and $T\,(-h/2) = T_0 + T_b$. Here, a stress-free state is assumed to exist at $T_0 = 300(K)$. The solution of the above differential Eq. (5) is

$$T(z) = T_0 + T_b - (T_t - T_b)\frac{\int_{-h/2}^{z} \frac{1}{k(z)}\mathrm{d}z}{\int_{-h/2}^{h/2} \frac{1}{k(z)}\mathrm{d}z} \tag{6}$$

In the case of power-law FG plate, the analytical solution of Eq. (6) can be obtained by means of polynomial series [30,38,48]

$$T(z) = T_b + \frac{(T_t - T_b)}{C_{tb}}\left[\left(\frac{2z+h}{2h}\right) - \frac{k_{tb}}{(p+1)k_b}\left(\frac{2z+h}{2h}\right)^{p+1} + \frac{k_{tb}^2}{(2p+1)k_b^2}\left(\frac{2z+h}{2h}\right)^{2p+1} - \frac{k_{tb}^3}{(3p+1)k_b^3}\left(\frac{2z+h}{2h}\right)^{3p+1} + \frac{k_{tb}^4}{(4p+1)k_b^4}\left(\frac{2z+h}{2h}\right)^{4p+1} - \frac{k_{tb}^5}{(5p+1)k_b^5}\left(\frac{2z+h}{2h}\right)^{5p+1}\right] \tag{7}$$

with

$$C_{tb} = 1 - \frac{k_{tb}}{(p+1)k_b} + \frac{k_{tb}^2}{(2p+1)k_b^2} - \frac{k_{tb}^3}{(3p+1)k_b^3} + \frac{k_{tb}^4}{(4p+1)k_b^4} - \frac{k_{tb}^5}{(5p+1)k_b^5} \tag{8}$$

where $k_{tb} = k_t - k_b$ with $k_t$and k_b are the thermal conductivity of the top and bottom surfaces of the plate, respectively.

2.2.4 Sinusoidal temperature rise

The sinusoidal temperature field used in this case is expressed as [30,49]

$$T(z) = T_0 + (T_t - T_b)\left[1 - \cos\left(\frac{\pi z}{2h} + \frac{\pi}{4}\right)\right] + T_b \tag{9}$$

2.3 Displacement fields and constitutive relations

Based on a 2D higher shear deformation theory, the displacement fields are expressed as follows

$$u(x, y, z, t) = u_0(x, y, t) - z\frac{\partial w_0}{\partial x} + k_1\, f(z)\int \theta\,(x, y, t)\,\mathrm{d}x \tag{10a}$$

$$v(x, y, z, t) = v_0(x, y, t) - z\frac{\partial w_0}{\partial y} + k_2\, f(z)\int \theta\,(x, y, t)\,\mathrm{d}y \tag{10b}$$

$$w(x, y, z, t) = w_0(x, y, t) \tag{10c}$$

where u_0, v_0 and w_0 are mid-plane displacements and θ is the rotation of normal to the mid-plane of the plate. $f(z)$ is a shear strain shape function defining the variation of the transverse shear strains and stresses across the thickness of the plate given in Eq. (11) [44].

$$f\,(z) = \frac{\pi h}{\pi^4 + h^4}e^{(hz/\pi)}\left(\pi^2 \sin\left(\frac{\pi z}{h}\right) + h^2\cos\left(\frac{\pi z}{h}\right)\right) - \frac{\pi h^3}{\pi^4 + h^4} \text{ and } g\,(z) = \frac{\mathrm{d}f}{\mathrm{d}z} \tag{11}$$

The suppositions in Eq. (10) are based on the application of linear, small-strain elasticity theory, from which the general strain— displacement relations are expressed as

$$\begin{Bmatrix}\varepsilon_x\\ \varepsilon_y\\ \gamma_{xy}\end{Bmatrix} = \begin{Bmatrix}\varepsilon_x^0\\ \varepsilon_y^0\\ \gamma_{xy}^0\end{Bmatrix} + z\begin{Bmatrix}k_x^b\\ k_y^b\\ k_{xy}^b\end{Bmatrix} + f(z)\begin{Bmatrix}k_x^s\\ k_y^s\\ k_{xy}^s\end{Bmatrix}, \begin{Bmatrix}\gamma_{yz}\\ \gamma_{xz}\end{Bmatrix} = g(z)\begin{Bmatrix}\gamma_{yz}^0\\ \gamma_{xz}^0\end{Bmatrix} \tag{12}$$

where

$$\left\{\begin{array}{c}\varepsilon_x^0\\ \varepsilon_y^0\\ \gamma_{xy}^0\end{array}\right\}=\left\{\begin{array}{c}\frac{\partial u_0}{\partial x}\\ \frac{\partial v_0}{\partial y}\\ \frac{\partial u_0}{\partial y}+\frac{\partial v_0}{\partial x}\end{array}\right\},\left\{\begin{array}{c}k_x^b\\ k_y^b\\ k_{xy}^b\end{array}\right\}=\left\{\begin{array}{c}-\frac{\partial^2 w_0}{\partial x^2}\\ -\frac{\partial^2 w_0}{\partial y^2}\\ -2\frac{\partial^2 w_0}{\partial x\partial y}\end{array}\right\}, \tag{13a}$$

$$\left\{\begin{array}{c}k_x^s\\ k_y^s\\ k_{xy}^s\end{array}\right\}=\left\{\begin{array}{c}k_1\theta\\ k_2\theta\\ k_1\frac{\partial}{\partial y}\int\theta\mathrm{d}x+k_2\frac{\partial}{\partial x}\int\theta\mathrm{d}y\end{array}\right\} \tag{13b}$$

$$\left\{\begin{array}{c}\gamma_{yz}^0\\ \gamma_{xz}^0\end{array}\right\}=\left\{\begin{array}{c}k_2\int\theta\mathrm{d}y\\ k_1\int\theta\mathrm{d}x\end{array}\right\},\ g(z)=\frac{\mathrm{d}f(z)}{\mathrm{d}z} \tag{13c}$$

The used integrals in the above equations were resolved using the Navier's method and written as

$$\frac{\partial}{\partial y}\int\theta\mathrm{d}x=A'\frac{\partial^2\theta}{\partial x\partial y},\quad\frac{\partial}{\partial x}\int\theta\mathrm{d}y=B'\frac{\partial^2\theta}{\partial x\partial y}, \tag{14a}$$

$$\int\theta\mathrm{d}x=A'\frac{\partial\theta}{\partial x},\quad\int\theta\mathrm{d}y=B'\frac{\partial\theta}{\partial y} \tag{14b}$$

where coefficientsA', $B'k_1$, $k_2$are expressed as follows

$$A'=-\frac{1}{\alpha^2},\quad B'=-\frac{1}{\beta^2},\quad k_1=\alpha^2,\quad k_2=\beta^2 \tag{15}$$

α and β are defined in Eq. (28).

The linear constitutive relations of FG plate are given below

$$\left\{\begin{array}{c}\sigma_x\\ \sigma_y\\ \tau_{yz}\\ \tau_{xz}\\ \tau_{xy}\end{array}\right\}=\left[\begin{array}{ccccc}Q_{11}&Q_{12}&0&0&0\\ Q_{12}&Q_{22}&0&0&0\\ 0&0&Q_{44}&0&0\\ 0&0&0&Q_{55}&0\\ 0&0&0&0&Q_{66}\end{array}\right]\left\{\begin{array}{c}\varepsilon_x\\ \varepsilon_y\\ \gamma_{yz}\\ \gamma_{xz}\\ \gamma_{xy}\end{array}\right\} \tag{16}$$

in which $(\sigma_x,\sigma_y,\tau_{xy},\tau_{yz},\tau_{xz})$ and $(\varepsilon_x,\varepsilon_y,\gamma_{xy},\gamma_{yz},\gamma_{xz})$ are the stresses and the strains components, respectively. The Q_{ij} expressions in terms of engineering constants determined using the material properties given in Eq. (1) are as follows

$$Q_{11}=Q_{22}=\frac{E\,(z,T)}{1-\nu^2\,(z,T)}, \tag{17a}$$

$$Q_{12}=\nu\,(z,T)\,Q_{11}, \tag{17b}$$

$$Q_{44}=Q_{55}=Q_{66}=\frac{E\,(z,T)}{2\,(1+\nu\,(z,T))} \tag{17c}$$

2.4 Plate governing equations

In order to obtain the governing differential equations, Hamilton's principle [50] is used.

$$\delta\int_0^t(U_M+U_T-K)\mathrm{d}t=0 \tag{18}$$

where U_M and U_T are the strain energies due to mechanical and thermal effects, respectively. K is the kinetic energy.

The strain energies U_M and U_T of the plate can be expressed by [30,51]

$$U_M = \frac{1}{2}\int_V \left[\sigma_x\varepsilon_x + \sigma_y\varepsilon_y + \tau_{xy}\gamma_{xy} + \tau_{yz}\gamma_{yz} + \tau_{xz}\gamma_{xz}\right] \mathrm{d}V \tag{19}$$

$$U_T = \frac{1}{2}\int_V \left\{\sigma_x^T\left[\left(\frac{\partial u}{\partial x}\right)^2 + \left(\frac{\partial v}{\partial x}\right)^2 + \left(\frac{\partial w}{\partial x}\right)^2\right] + \sigma_y^T\left[\left(\frac{\partial u}{\partial y}\right)^2 + \left(\frac{\partial v}{\partial y}\right)^2 + \left(\frac{\partial w}{\partial y}\right)^2\right]\right\} \mathrm{d}V \tag{20}$$

with

$$\sigma_x^T = -\left(Q_{11} + Q_{12}\right)\alpha(z,T)\Delta T(z) \text{ and } \sigma_y^T = -\left(Q_{22} + Q_{12}\right)\alpha(z,T)\Delta T(z) \tag{21}$$

The kinetic energy of the plate is given by the following form:

$$K = \frac{1}{2}\int_V \rho(z,T)\left[\dot{u}^2 + \dot{v}^2 + \dot{w}^2\right] \mathrm{d}V \tag{22}$$

By using Eqs. (10), (12), (16), substituting the expressions of Eqs. (19), (20), (22) into Eq. (18), integrating the displacement gradients by parts and setting the coefficients of δu_0, δv_0, δw_0, $\delta\theta$ to zero independently. The differential equations of motion for FG plate can be obtained as follows:

$$\begin{aligned}
\delta u_0 \;:\; & \left(A_{11} + A_{11}^T\right) d_{11}u_0 + \left(A_{66} + A_{22}^T\right) d_{22}u_0 + \left(A_{12} + A_{66}\right) d_{12}v_0 \\
& - \left(B_{11} + B_{11}^T\right) d_{111}w_0 - \left(B_{12} + 2B_{66} + B_{22}^T\right) d_{122}w_0 + k_1A'(B_{11}^s + B_{11}^{sT})d_{111}\theta \\
& + \left(k_2B'B_{12}^s + (k_1A' + k_2B')B_{66}^s + k_1A'B_{22}^{sT}\right) d_{122}\theta = I_0\ddot{u}_0 - I_1d_1\ddot{w}_0 + (k_1A')J_1d_1\ddot{\theta}
\end{aligned} \tag{23a}$$

$$\begin{aligned}
\delta v_0 \;:\; & \left(A_{12} + A_{66}\right) d_{12}u_0 + \left(A_{66} + A_{11}^T\right) d_{11}v_0 + \left(A_{22} + A_{22}^T\right) d_{22}v_0 \\
& - \left(B_{12} + 2B_{66} + B_{11}^T\right) d_{112}w_0 - (B_{22} + B_{22}^T)d_{222}w_0 + k_2B'\left(B_{22}^s + B_{22}^{sT}\right) d_{222}\theta \\
& + \left(k_1A'B_{12}^s + (k_1A' + k_2B')B_{66}^s + k_2B'B_{11}^{sT}\right) d_{112}\theta = I_0\ddot{v}_0 - I_1d_2\ddot{w}_0 + J_1k_2B'd_2\ddot{\theta}
\end{aligned} \tag{23b}$$

$$\begin{aligned}
\delta w_0 \;:\; & \left(B_{11} + B_{11}^T\right) d_{111}u_0 + \left(B_{12} + 2B_{66} + B_{22}^T\right) d_{122}u_0 + \left(B_{12} + 2B_{66} + B_{11}^T\right) d_{112}v_0 \\
& + \left(B_{22} + B_{22}^T\right) d_{222}v_0 - \left(D_{11} + D_{11}^T\right) d_{1111}w_0 - \left(2D_{12} + 4D_{66} + D_{11}^T + D_{22}^T\right) d_{1122}w_0 \\
& - \left(D_{22} + D_{22}^T\right) d_{2222}w_b + A_{11}^T d_{11}w_0 + A_{22}^T d_{22}w_0 + k_1A'\left(D_{11}^s + D_{11}^{sT}\right) d_{1111}\theta \\
& - \left(k_1A' + k_2B'\right)\left(D_{12}^s + 2D_{66}^s\right) d_{1122}\theta + \left(k_2B'D_{11}^{sT} + k_1A'D_{22}^{sT}\right) d_{1122}\theta \\
& + k_2B'\left(D_{22}^s + D_{22}^{sT}\right) d_{2222}\theta = I_0\ddot{w}_0 + J_0\ddot{\phi}_z + I_1\left(d_1\ddot{u}_0 + d_2\ddot{v}_0\right) - I_2\nabla^2\ddot{w}_0 \\
& + J_2\left(k_1A'd_{11}\ddot{\theta} + k_2B'd_{22}\ddot{\theta}\right)
\end{aligned} \tag{23c}$$

$$\begin{aligned}
\delta\theta \;:\; & k_1A'\left(B_{11}^s + B_{11}^{sT}\right) d_{111}u_0 + \left(k_2B'B_{12}^s + \left(k_1A' + k_2B'\right)B_{66}^s + k_1A'B_{22}^{sT}\right) d_{122}u_0 \\
& + \left(k_1A'B_{12}^s + \left(k_1A' + k_2B'\right)B_{66}^s + k_2B'B_{11}^{sT}\right) d_{112}v_0 + k_2B'\left(B_{22}^s + B_{22}^{sT}\right) d_{222}v_0 \\
& - k_1A'\left(D_{11}^s + D_{11}^{sT}\right) d_{1111}w_0 - \left(k_1A' + k_2B'\right)\left(D_{12}^s + 2D_{66}^s\right) d_{1122}w_0 \\
& - \left(k_2B'D_{11}^{sT} + k_1A'D_{22}^{sT}\right) d_{1122}w_0 - k_2B'\left(D_{22}^s + D_{22}^{sT}\right) d_{2222}w_0 - \left(k_1A'\right)^2\left(H_{11}^s + H_{11}^{sT}\right) d_{1111}\theta - \\
& \left(2k_1A'k_2B'H_{12}^s + \left(k_1A' + k_2B'\right)^2 H_{66}^s + \left(k_2B'\right)^2 H_{11}^{sT} + \left(k_1A'\right)^2 H_{22}^{sT}\right) d_{1122}\theta \\
& - \left(k_2B'\right)^2\left(H_{22}^s + H_{22}^{sT}\right) d_{2222}\theta + (k_1A')^2A_{55}^s d_{11}\theta \;\; + (k_2B')^2A_{44}^s d_{22}\theta = \\
& - J_1\left(k_1A'd_1\ddot{u}_0 + k_2B'd_2\ddot{v}_0\right) + J_2\left(k_1A'd_{11}\ddot{w}_0 + k_2B'd_{22}\ddot{w}_0\right) - K_2\left((k_1A')^2d_{11}\ddot{\theta} + (k_2B')^2d_{22}\ddot{\theta}\right)
\end{aligned} \tag{23d}$$

where d_{ij}, d_{ijl} and d_{ijlm} are the following differential operators:

$$d_{ij} = \frac{\partial^2}{\partial x_i\partial x_j}, \quad d_{ijl} = \frac{\partial^3}{\partial x_i\partial x_j\partial x_l}, \quad d_{ijlm} = \frac{\partial^4}{\partial x_i\partial x_j\partial x_l\partial x_m}, \quad d_i = \frac{\partial}{\partial x_i}, \quad (i,j,l,m = 1,2). \tag{24}$$

and stiffness components are given as:

$$\begin{Bmatrix} A_{11} & B_{11} & D_{11} & B_{11}^s & D_{11}^s & H_{11}^s \\ A_{12} & B_{12} & D_{12} & B_{12}^s & D_{12}^s & H_{12}^s \\ A_{66} & B_{66} & D_{66} & B_{66}^s & D_{66}^s & H_{66}^s \end{Bmatrix} = \int_{-h/2}^{h/2} C_{11}\left(1, z, z^2, f(z), zf(z), f^2(z)\right) \begin{Bmatrix} 1 \\ \nu \\ \frac{1-\nu}{2} \end{Bmatrix} \mathrm{d}z, \tag{25a}$$

$$\left(A_{22}, B_{22}, D_{22}, B^s_{22}, D^s_{22}, H^s_{22}\right) = \left(A_{11}, B_{11}, D_{11}, B^s_{11}, D^s_{11}, H^s_{11}\right), \tag{25b}$$

$$A^s_{44} = A^s_{55} = \int_{-h/2}^{h/2} C_{44}\,[g(z)]^2\,\mathrm{d}z, \tag{25c}$$

$$\begin{Bmatrix} A^T_{11} & B^T_{11} & D^T_{11} & B^{sT}_{11} & D^{sT}_{11} & H^{sT}_{11} \\ A^T_{22} & B^T_{22} & D^T_{22} & B^{sT}_{22} & D^{sT}_{22} & H^{sT}_{22} \end{Bmatrix} = \int_{-h/2}^{h/2} \left(1, z, z^2, f(z), zf(z), f(z)^2\right) \begin{Bmatrix} \sigma^T_x \\ \sigma^T_y \end{Bmatrix} \mathrm{d}z \tag{25d}$$

The inertias are also defined as:

$$(I_0, I_1, J_1, I_2, J_2, K_2) = \int_{-h/2}^{h/2} \left(1, z, f, z^2, zf, f^2\right) \rho(z)\mathrm{d}z \tag{26}$$

2.5 Analytical solutions

In order to solve Eq. (23), the Navier's method is adopted to satisfy simply supported boundary conditions. So that, the analytical solutions are expressed based on double-Fourier series as presented below:

$$\begin{Bmatrix} u_0 \\ v_0 \\ w_0 \\ \theta \end{Bmatrix} = \sum_{m=1}^{\infty}\sum_{n=1}^{\infty} \begin{Bmatrix} U_{mn}\, e^{i\omega t} \cos(\alpha x)\sin(\beta y) \\ V_{mn}\, e^{i\omega t} \sin(\alpha x)\cos(\beta y) \\ W_{mn}\, e^{i\omega t} \sin(\alpha x)\sin(\beta y) \\ \theta_{mn}\, e^{i\omega t} \sin(\alpha x)\sin(\beta y) \end{Bmatrix} \tag{27}$$

where U_{mn}, V_{mn}, W_{mn} and θ_{mn} are arbitrary parameters to be determined, ω is the Eigen-frequency associated with (m,n) the Eigen-mode. α and β are stated as:

$$\alpha = m\pi/a \text{ and } \beta = n\pi/b. \tag{28}$$

Substituting Eq. (27) into Eq. (23), the following eigenvalue equation is found:

$$\left(\begin{bmatrix} s_{11} & s_{12} & s_{13} & s_{14} \\ s_{12} & s_{22} & s_{23} & s_{24} \\ s_{13} & s_{23} & s_{33} & s_{34} \\ s_{14} & s_{24} & s_{34} & s_{44} \end{bmatrix} - \omega^2 \begin{bmatrix} m_{11} & 0 & m_{13} & m_{14} \\ 0 & m_{22} & m_{23} & m_{24} \\ m_{13} & m_{23} & m_{33} & m_{34} \\ m_{14} & m_{24} & m_{34} & m_{44} \end{bmatrix} \right) = \begin{Bmatrix} 0 \\ 0 \\ 0 \\ 0 \end{Bmatrix} \tag{29}$$

in which:

$$\begin{aligned}
s_{11} &= -\alpha^2\left(A_{11} + A^T_{11}\right) - \lambda^2\left(A_{66} + A^T_{22}\right) \\
s_{12} &= -\alpha\beta\left(A_{12} + A_{66}\right) \\
s_{13} &= \alpha\left[\alpha^2\left(B_{11} + B^T_{11}\right) + \beta^2\left(B_{12} + 2B_{66} + B^T_{22}\right)\right] \\
s_{14} &= -k_1A'\alpha^3\left(B^s_{11} + B^{sT}_{11}\right) - \alpha\beta^2\left(k_2B'B^s_{12} + (k_1A' + k_2B')B^s_{66} + k_1A'B^{sT}_{22}\right) \\
s_{22} &= -\alpha^2\left(A_{66} + A^T_{11}\right) - \beta^2\left(A_{22} + A^T_{22}\right) \\
s_{23} &= \beta\left[\alpha^2\left(B_{12} + 2B_{66} + B^T_{11}\right) + \beta^2(B_{22} + B^T_{22})\right] \\
s_{24} &= -\beta\left[\beta^2k_2B'\left(B^s_{22} + B^{sT}_{22}\right) + \alpha^2\left(k_1A'B^s_{12} + (k_1A' + k_2B')B^s_{66} + k_2B'B^{sT}_{11}\right)\right] \\
s_{33} &= -\left[\left(D_{11} + D^T_{11}\right)\alpha^4 + \left(D_{22} + D^T_{22}\right)\beta^4 + \left(2D_{12} + 4D_{66} + D^T_{22} + D^T_{11}\right)\alpha^2\beta^2 + A^T_{11}\alpha^2 + A^T_{22}\beta^2\right] \\
s_{34} &= k_1A'\left(D^s_{11} + D^{sT}_{11}\right)\alpha^4 - \left(k_1A' + k_2B'\right)\left(D^s_{12} + 2D^s_{66}\right)\alpha^2\beta^2 + \left(k_1A'D^{sT}_{11} + k_2B'D^{sT}_{22}\right)\alpha^2\beta^2 \\
&\quad + k_2B'\left(D^s_{22} + D^{sT}_{22}\right)\mu^4 \\
s_{44} &= -\left(k_1A'\right)^2\left(H^s_{11} + H^{sT}_{11}\right)\alpha^4 - \left(2k_1A'k_2B'H^s_{12} + \left(k_1A' + k_2B'\right)^2H^s_{66} + \left(k_2B'\right)^2H^{sT}_{11} + \left(k_1A'\right)^2H^{sT}_{22}\right)\alpha^2\beta^2 \\
&\quad - \left(k_2B'\right)^2\left(H^s_{22} + H^{sT}_{22}\right)\beta^4 - (k_1A')^2\alpha^2A^s_{55} - (k_2B')^2\beta^2A^s_{44}
\end{aligned} \tag{30a}$$

$$\begin{aligned}
&m_{11} = m_{22} = I_0, \quad m_{12} = 0 \\
&m_{13} = -\alpha\, I_1, \quad m_{14} = \alpha\, k_1A'\, J_1, \quad m_{23} = -\beta\, I_1 \\
&m_{24} = \beta\, k_2B'\, J_1, \quad m_{33} = I_0 + I_2(\alpha^2 + \beta^2), \quad m_{34} = -J_2(k_1A'\alpha^2 + k_2B'\beta^2) \\
&m_{44} = K_2((k_1A')^2\alpha^2 + (k_2B')^2\beta^2).
\end{aligned} \tag{30b}$$

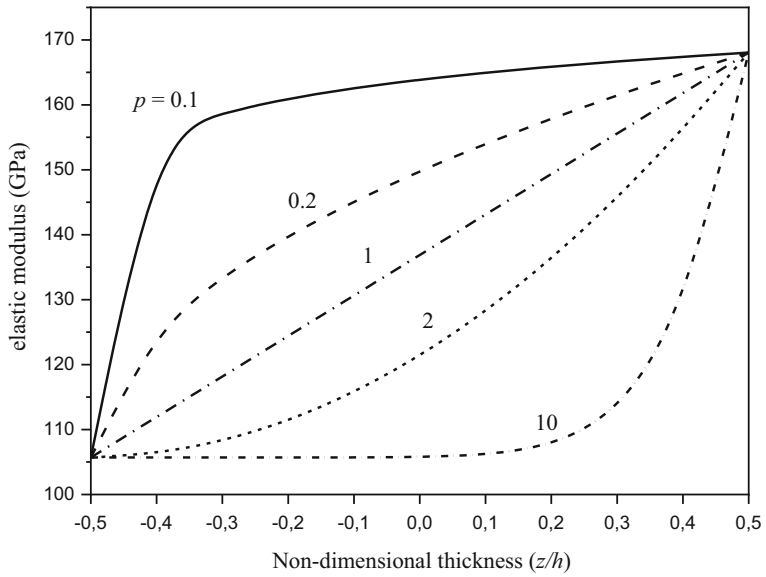

Fig. 2 Variation of elastic modulus versus non-dimensional thickness (z/h) of FG plate in room temperature field and different values of power law index (p)

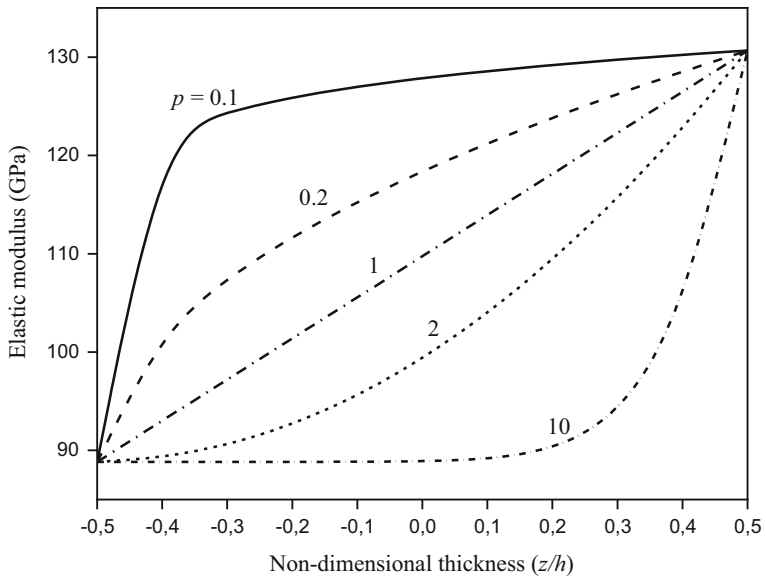

Fig. 3 Variation of elastic modulus versus non-dimensional thickness (z/h) of FG plate in linear temperature field and different values of power law index (p)

3 Results and discussion

Various numerical results calculated using the present theory are presented in this section for temperature-dependent FG plates by considering two different types of FG plates such as $ZrO_2/Ti-6Al-4V$ and $Si_3N_4/SUS304$ (see Table 1). The non-dimensional frequency parameter is taken as [22,30].

$$\overline{\omega} = \omega(a^2/h)\left[\rho_b(1-\nu^2)/E_b\right]^{1/2} \tag{31}$$

where E_b and ρ_b are at $T_0 = 300(K)$.

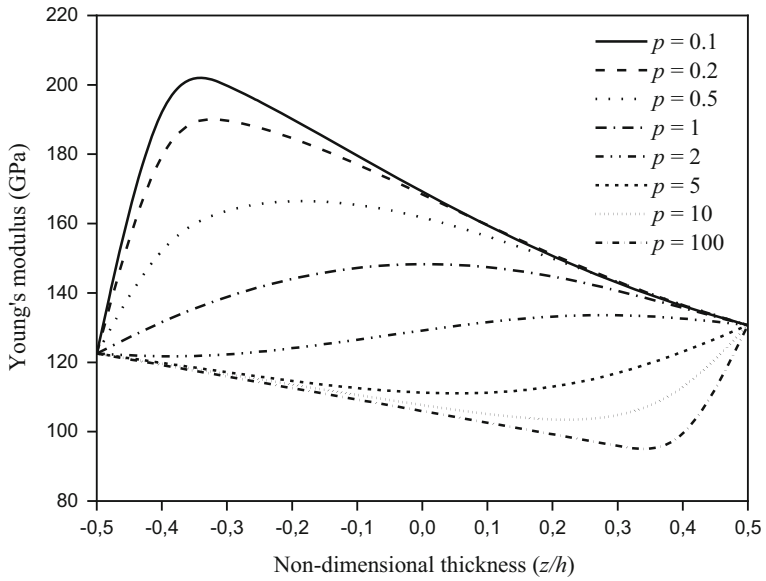

Fig. 4 Variation of elastic modulus versus non-dimensional thickness (z/h) of FG plate in nonlinear temperature field and different values of power law index (p)

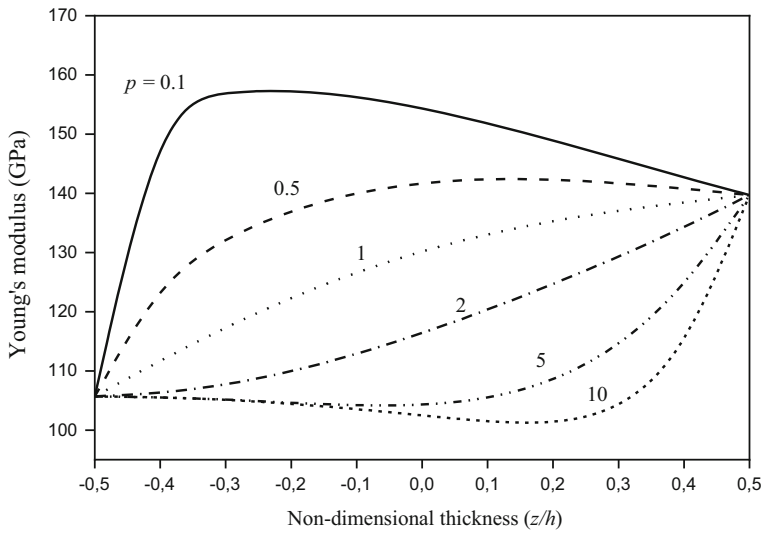

Fig. 5 Variation of elastic modulus versus non-dimensional thickness (z/h) of FG plate in sinusoidal temperature field and different values of power law index (p)

3.1 Material properties in thermal conditions

The variation of Young modulus across the thickness of FG plates subjected to a uniform (room temperature), linear, nonlinear and sinusoidal thermal conditions is presented in Figs. 2 to 6, respectively. Room temperature is defined as $T_0 = 300(K)$ for all thermal conditions. The temperature rise in linear form is $T_b = T_t = 600(K)$, the nonlinear thermal conditions are $T_b = 0(K)$ and $T_t = 600(K)$ and the sinusoidal thermal conditions are $T_b = 300(K)$ and $T_t = 500(K)$.

Figure 2 and 3 present the variation of the elastic modulus through the thickness in uniform and sinusoidal thermal loads, respectively. It can be seen that the variations of Young's modulus are similar in the two cases, but the curves move to smaller values with the linear temperature load. It is also clear that the increase of the power law index leads to the decrease of the Young's modulus. For nonlinear and sinusoidal thermal loads, the values of Young's modulus as shown in Figs. 4 and 5 increase close to the lower surface then decrease

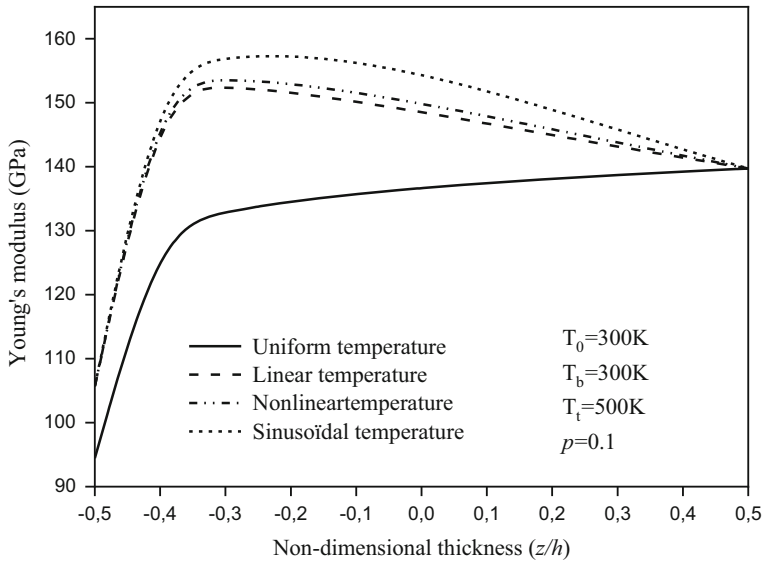

Fig. 6 Variation of elastic modulus versus non-dimensional thickness (z/h) of FG plate in uniform, linear, nonlinear and sinusoidal temperature field and different values of power law index (p)

when $p \leqslant 1$. On the other hand, they decrease then increase close to the upper surface when $p > 1$. In Fig. 6, a comparison study on Young's modulus is undertaken for uniform, linear, nonlinear and sinusoidal thermal conditions. From these figures, it can be concluded that the behavior of Young's modulus in uniform and linear thermal conditions is completely different from that in nonlinear and sinusoidal temperature cases, which means that the environmental conditions type affect considerably the variation of the elastic modulus.

3.2 Numerical results and validation

In order to prove and validate the efficiency of this theory, the non-dimensional natural frequencies are calculated for temperature-dependent and temperature-independent FG plates and they are compared with those obtained by Shahrjerdi et al. [30] using a second-order shear deformation theory (SSDT), Huang and Shen [22] based on a third-order shear deformation theory (TSDT) and Attia et al. [38] using four variables higher-order shear deformation theory (third plate theory (TPT), sinusoidal plate theory (SPT), hyperbolic plate theory (HPT), exponential plate theory (EPT) as presented in Table 2 and 3, respectively. Verifications are implemented by supposing the following conditions parameters: $h = 0.025$ m, $a = b = 0.2$ m.

In Table 2, a FG plate made of $ZrO_2/Ti{-}6Al{-}4V$ is analyzed. In this example, Young's modulus and thermal expansion coefficient of these materials are considered to be temperature-dependent [22,30]. However, a same value of Poisson's ratio ν for both ceramic and metal is supposed to be $\nu = 0.3$. From this Table, it can be seen that the comparison of non-dimensional natural frequencies is carried out for different values of power law index and thermal conditions loads (temperature-dependent and temperature-independent) FG plates (FGP). Therefore, the obtained results using the present theory are found to be in very good agreement with the results of Attia et al. [38] using various efficient higher-order shear deformation theories (TPT, SPT, HPT and EPT) Huang and Shen [22] and Shahrjerdi et al. [30].

In Table 3, comparisons are made using a FG $Si_3N_4/SUS304$ plate. For these materials, the Poisson's ratio is taken $\nu = 0.28$. The computed dimensionless fundamental frequencies are compared with those given by Attia et al. [38], Shahrjerdi et al [30] and Huang and Shen [22] in Table 4 for different values of power law index p. As a result, this comparison shows that the present results are in very good agreement with existing results for all values of power law index p, either for the case of temperature-dependent and temperature-independent FG plates (FGP).

In the next example, a $ZrO_2/Ti{-}6Al{-}4V$ and $Si_3N_4/SUS304$ plates are considered and the obtained results are compared to those of Huang and Shen [22] and Shahrjerdi et al. [30] as shown in Tables 4 and 5, respectively. It can be seen that the computed results are in good agreement with the previously published results [22,30] and these for different considered shape mode.

Table 2 Non-dimensional natural frequencies of simply supported (ZrO_2/Ti−6Al−4V) FG plate in thermal environments

Mode (1,1) Natural frequency of FGP (ZrO_2 and Ti−6Al−4V)	$T_b = 300(K)$				
	$T_t = 300(K)$	$T_t = 400(K)$		$T_t = 600(K)$	
		Temperature-dependent	Temperature-independent	Temperature-dependent	Temperature-independent
ZrO_2					
SSDT[a]	8.333	7.614	7.892	5.469	6.924
TSDT[b]	8.273	7.868	8.122	6.685	7.686
TPT[c]	8.278	7.807	8.130	6.533	7.826
SPT[c]	8.278	7.808	8.131	6.534	7.826
HPT[c]	8.278	7.808	8.131	6.534	7.826
EPT[c]	8.280	7.809	8.132	6.536	7.828
Present method	**8.281**	**7.810**	**8.061**	**6.536**	**7.604**
$p = 0.5$					
SSDT[a]	7.156	6.651	6.844	5.255	6.175
TSDT[b]	7.139	6.876	7.154	6.123	6.776
TPT[c]	7.111	6.781	7.005	5.931	6.789
SPT[c]	7.112	6.782	7.006	5.931	6.789
HPT[c]	7.112	6.782	7.006	5.931	6.789
EPT[c]	7.113	6.783	7.001	5.993	6.772
Present method	**7.113**	**6.784**	**6.962**	**5.933**	**6.648**
$p = 1$					
SSDT[a]	6 .700	6.281	6.446	5.167	5.904
TSDT[b]	6.657	6.437	6.592	5.819	6.362
TPT[c]	6.657	6.375	6.565	5.664	6.378
SPT[c]	6.657	6.375	6.565	5.665	6.378
HPT[c]	6.657	6.375	6.565	5.665	6.378
EPT[c]	6.658	6.376	6.556	5.668	6.350
Present method	**6.659**	**6.377**	**6.531**	**5.667**	**6.267**
$p = 2$					
SSDT[a]	6.333	5.992	6.132	5.139	5.711
TSDT[b]	6.286	6.101	6.238	5.612	6.056
TPT[c]	6.287	6.047	6.208	5.467	6.049
SPT[c]	6.287	6.047	6.208	5.467	6.049
HPT[c]	6.287	6.047	6.208	5.467	6.049
EPT[c]	6.288	6.049	6.194	5.469	6.003
Present method	**6.289**	**6.049**	**6.184**	**5.469**	**5.968**
Ti–6Al–4V					
SSDT[a]	5.439	5.103	5.333	4.836	5.115
TSDT[b]	5.400	5.322	5.389	5.118	5.284
TPT[c]	5.403	5.303	5.361	5.132	5.275
SPT[c]	5.403	5.303	5.361	5.132	5.275
HPT[c]	5.403	5.303	5.361	5.132	5.275
EPT[c]	5.404	5.304	5.300	5.133	5.091
Present method	**5.405**	**5.303**	**5.362**	**5.130**	**5.274**

Bold values used in this table is just to differenciate between the obtained results and the others

[a] Shahrjerdi et al. [30]

[b] Huang and Shen [22]

[c] Attia et al. [38]

In what follow, the non-dimensional natural frequencies are calculated using the expression as written below:

$$\overline{\omega} = \omega(b^2/\pi^2)\,[I_0/D_0]^{1/2} \tag{32}$$

where $I_0 = \rho h$ and $D_0 = Eh^3/12(1-\nu^2)$

The variation of the first-four dimensionless frequencies of simply supported square FG plate made of ZrO_2/Ti−6Al−4V subjected to a uniform (room temperature), linear, nonlinear and sinusoidal thermal loads is shown in Figs. 7 to 10, respectively. The results show that natural frequencies reduce with the increase in

Table 3 Non-dimensional natural frequencies of simply supported (Si_3N_4/SUS304) FG plate in thermal environments

Mode (1,1) Natural frequency of FGP (Si_3N_4 and SUS304)	$T_b = 300(K)$				
	$T_t = 300(K)$	$T_t = 400(K)$		$T_t = 600(K)$	
		Temperature-dependent	Temperature-independent	Temperature-dependent	Temperature-independent
Si_3N_4					
SSDT[a]	12.506	12.175	12.248	11.461	11.716
TSDT[b]	12.495	12.397	12.382	11.984	12.213
TPT[c]	12.507	12.307	12.376	11.886	12.113
SPT[c]	12.507	12.307	12.378	11.887	12.114
HPT[c]	12.507	12.307	12.378	11.886	12.114
EPT[c]	12.509	12.309	12.380	11.889	12.116
Present method	**12.508**	**12.308**	**12.378**	**11.887**	**12.114**
$p = 0.5$					
SSDT[a]	8.652	8.361	8.405	7.708	7.887
TSDT[b]	8.675	8.615	8.641	8.269	8.425
TPT[c]	8.609	8.453	8.498	8.117	8.272
SPT[c]	8.609	8.453	8.499	8.118	8.273
HPT[c]	8.609	8.453	8.499	8.118	8.273
EPT[c]	8.611	8.455	8.500	8.120	8.274
Present method	**8.610**	**8.454**	**8.499**	**8.119**	**8.273**
$p = 1$					
SSDT[a]	7.584	7.306	7.342	6.674	6.834
TSDT[b]	7.555	7.474	7.514	7.171	7.305
TPT[c]	7.544	7.399	7.437	7.082	7.217
SPT[c]	7.544	7.399	7.437	7.082	7.218
HPT[c]	7.544	7.399	7.437	7.082	7.218
EPT[c]	7.546	7.401	7.439	7.083	7.219
Present method	**7.545**	**7.399**	**7.437**	**7.082**	**7.218**
$p = 2$					
SSDT[a]	6.811	6.545	6.575	5.929	6.077
TSDT[b]	6.777	6.693	6.728	6.398	6.523
TPT[c]	6.771	6.631	6.664	6.323	6.447
SPT[c]	6.770	6.631	6.665	6.323	6.447
HPT[c]	6.770	6.631	6.665	6.323	6.447
EPT[c]	6.772	6.633	6.665	6.324	6.448
Present method	**6.771**	**6.632**	**6.665**	**6.323**	**6.447**
SUS304					
SSDT[a]	5.410	5.161	5.178	4.526	4.682
TSDT[b]	5.405	5.311	5.335	4.971	5.104
TPT[c]	5.410	5.272	5.295	4.922	5.055
SPT[c]	5.410	5.278	5.300	4.945	5.071
HPT[c]	5.410	5.278	5.299	4.945	5.071
EPT[c]	5.411	5.279	5.301	4.946	5.073
Present method	**5.411**	**5.279**	**5.300**	**4.945**	**5.072**

Bold values used in this table is just to differenciate between the obtained results and the others

[a] Shahrjerdi et al. [30]

[b] Huang and Shen [22]

[c] Attia et al. [38]

temperature which is due to the decreasing of elastic modulus with the temperature raise. Also, the decrease of the frequencies in the higher modes is important compared to that in the smaller modes. At the same field of temperature, the difference between two consecutive higher modes is less than that of the case of two successive lower modes. It is obvious that the effect of the temperature distribution in the case of a uniform thermal field is more significant compared to the other thermal conditions, this can be explained by the fact that the decrease of the frequency under linear thermal loadings, nonlinear and sinusoidal is almost identical, while the decrease in frequency is important in the case of a uniform thermal loading.

Table 4 Non-dimensional natural frequency parameter of simply supported (ZrO_2/Ti–6Al–4V) FG plate in thermal environments($p = 2$)

Mode numbers of FGP (ZrO_2 and Ti–6Al–4V)	$T_b = 300(K)$ $T_t = 300(K)$	$T_t = 400(K)$		$T_t = 600(K)$	
		Temperature-Dependent	Temperature-Independent	Temperature-Dependent	Temperature-Independent
(1,1)					
SSDT[a]	6.333	5.992	6.132	5.139	5.711
TSDT[b]	6.286	6.101	6.238	5.612	6.056
TPT[c]	6.287	6.047	6.208	5.467	6.049
SPT[c]	6.287	6.047	6.208	5.467	6.049
HPT[c]	6.287	6.047	6.208	5.467	6.049
EPT[c]	6.288	6.049	6.194	5.469	6.003
Present method	**6.289**	**6.049**	**6.184**	**5.469**	**5.968**
(1,2)					
SSDT[a]	14.896	14.383	14.684	13.260	14.253
TSDT[b]	14.625	14.372	14.655	13.611	14.474
TPT[c]	14.665	14.265	14.581	13.416	14.412
SPT[c]	14.666	14.267	14.583	13.416	14.414
HPT[c]	14.665	14.265	14.581	13.413	14.413
EPT[c]	14.672	14.273	14.589	13.421	14.420
Present method	**14.670**	**14.271**	**14.558**	**13.419**	**14.331**
(2,2)					
SSDT[a]	22.608	21.942	22.386	20.557	21.935
TSDT[b]	21.978	21.653	22.078	20.652	21.896
TPT[c]	22.123	21.584	22.034	20.489	21.855
SPT[c]	22.127	21.589	22.038	20.494	21.860
HPT[c]	22.123	21.584	22.034	20.489	21.855
EPT[c]	22.140	21.602	22.052	20.507	21.873
Present method	**22.133**	**21.595**	**22.014**	**20.499**	**21.774**
(1,3)					
SSDT[a]	27.392	26.630	27.163	25.077	26.700
TSDT[b]	26.454	26.113	26.605	24.961	26.435
TPT[c]	26.704	26.081	26.612	24.837	26.427
SPT[c]	26.711	26.089	26.619	24.845	26.435
HPT[c]	26.704	26.081	26.612	24.837	26.427
EPT[c]	26.731	26.108	26.639	24.865	26.454
Present method	**26.718**	**26.096**	**26.595**	**24.852**	**26.346**
(2,3)					
SSDT[a]	34.106	33.211	33.867	31.425	33.384
TSDT[b]	32.659	32.239	32.840	30.904	32.664
TPT[c]	33.109	32.371	33.013	30.920	32.819
SPT[c]	33.121	32.384	33.025	30.933	32.831
HPT[c]	33.109	32.370	33.013	30.919	32.819
EPT[c]	33.151	32.413	33.055	30.964	32.862
Present method	**33.130**	**32.392**	**33.000**	**31.941**	**32.740**

Bold values used in this table is just to differenciate between the obtained results and the others

[a] Shahrjerdi et al. [30]

[b] Huang and Shen [22]

[c] Attia et al. [38]

3.3 Parametric study

In this section, the effects of different parameters such as the power law index, the mode numbers, plate geometry, and temperature fields on the frequency of FG plates are investigated here.

The non-dimensional frequencies values are listed in Tables 6 and 7 for FG $ZrO_2/Ti-6Al-4V$ and Si_3N_4/SUS304 plates, respectively. The non-dimensional natural frequency parameter is defined as $\overline{\omega} = \omega(a^2/h)\left[\rho_b(1-\nu^2)/E_b\right]^{1/2}$, where E_b and ρ_b are at $T_0 = 300(K)$. The effect of power law index p on

Table 5 Non-dimensional natural frequency parameter of simply supported (Si_3N_4/SUS304) FG plate in thermal environments ($p = 2$)

Mode numbers of FGP (Si_3N_4/SUS304)	$T_b = 300(K)$ $T_t = 300(K)$	$T_t = 400(K)$		$T_t = 600(K)$	
		Temperature-dependent	Temperature-independent	Temperature-dependent	Temperature-independent
(1,1)					
SSDT[a]	6.811	6.445	6.575	5.929	6.077
TSDT[b]	6.777	6.693	6.728	6.398	6.523
TPT[c]	6.770	6.631	6.664	6.323	6.447
SPT[c]	6.770	6.631	6.664	6.323	6.447
HPT[c]	6.770	6.631	6.664	6.323	6.447
EPT[c]	6.770	6.631	6.665	6.325	6.448
Present method	**6.771**	**6.632**	**6.665**	**6.323**	**6.447**
(1,2)					
SSDT[a]	16.017	15.708	15.769	15.002	15.262
TSDT[b]	15.809	15.762	15.836	15.384	15.632
TPT[c]	15.812	15.628	15.699	15.229	15.472
SPT[c]	15.814	15.631	15.702	15.231	15.474
HPT[c]	15.812	15.628	15.699	15.229	15.472
EPT[c]	15.820	15.636	15.707	15.237	15.480
Present method	**15.814**	**15.631**	**15.702**	**15.231**	**15.474**
(2,2)					
SSDT[a]	24.307	23.958	24.047	23.154	23.517
TSDT[b]	23.806	23.786	23.893	23.327	23.685
TPT[c]	23.874	23.652	23.755	23.167	23.517
SPT[c]	23.879	23.657	23.760	23.173	23.522
HPT[c]	23.874	23.652	23.755	23.167	23.516
EPT[c]	23.893	23.671	23.774	23.187	23.536
Present method	**23.879**	**23.657**	**23.761**	**23.173**	**23.522**
(1,3)					
SSDT[a]	29.446	29.071	29.177	28.204	28.632
TSDT[b]	28.687	28.686	28.816	28.185	28.609
TPT[c]	28.831	28.586	28.709	28.049	28.463
SPT[c]	28.839	28.594	28.717	28.057	28.471
HPT[c]	28.831	28.586	28.709	28.049	28.462
EPT[c]	28.860	28.614	28.738	28.078	28.491
Present method	**28.839**	**28.594**	**28.717**	**28.058**	**28.471**
(2,3)					
SSDT[a]	36.657	36.247	36.376	35.290	35.809
TSDT[b]	35.466	35.491	35.648	34.918	35.436
TPT[c]	35.768	35.489	35.640	34.879	35.383
SPT[c]	35.782	35.503	35.654	34.893	35.397
HPT[c]	35.768	35.489	35.640	34.878	35.383
EPT[c]	35.814	35.535	35.686	34.925	35.429
Present method	**35.782**	**35.503**	**35.654**	**34.893**	**35.397**

Bold values used in this table is just to differenciate between the obtained results and the others

[a] Shahrjerdi et al. [30]

[b] Huang and Shen [22]

[c] Attia et al. [38]

the frequencies can be seen by considering the same value of thermal load and shape mode. The results for FG plates are found to be between those for pure material plates, since Young's modulus increases from pure metal to pure ceramic. The frequencies decrease by increasing the temperature difference between top and bottom surfaces for the same value of power law index and shape mode that represent the effects of thermal loads. The comparison between temperature-dependent and independent FG plates in Tables 6 and 7 reveals the smaller frequencies in temperature-dependent FG plates, which proves the accuracy and effectiveness of temperature-dependent material properties.

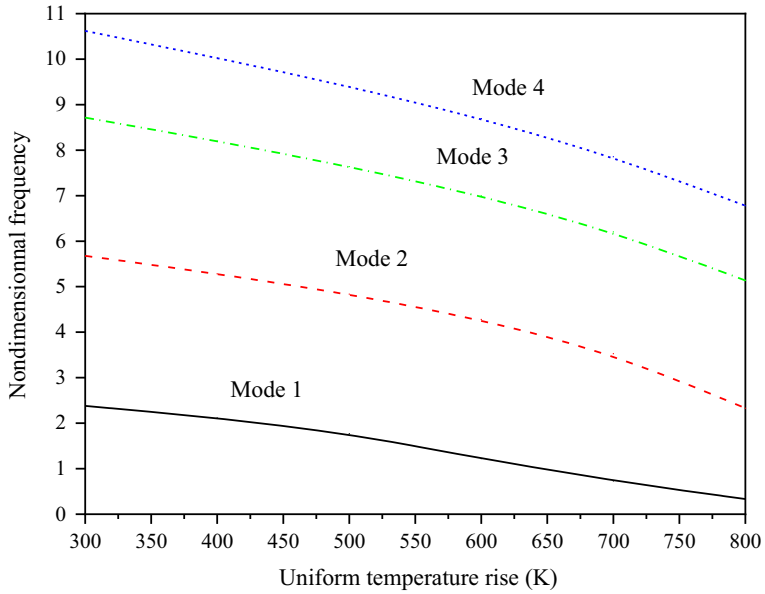

Fig. 7 First four Non-dimensional frequency parameters versus uniform temperature field for simply supported (ZrO_2/Ti−6Al−4V) FGP when $(a/h = 10)$, $(a = 0.2)$, $(p = 1)$

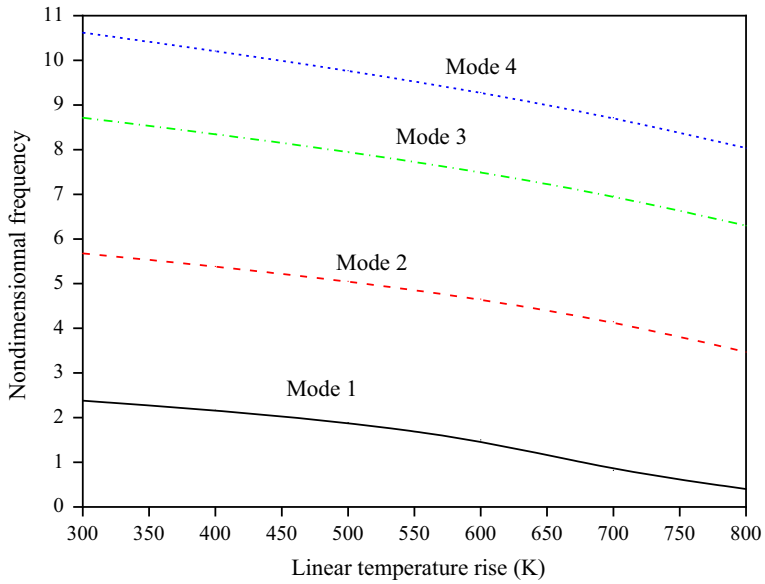

Fig. 8 First four Non-dimensional frequency parameters versus linear temperature field for simply supported (ZrO_2/Ti−6Al−4V) FGP when $(a/h = 10)$, $(a = 0.2)$, $(p = 1)$

In Figs. 11, 12, 13 and 14, the effect of side-to-side ratio on the variation of dimensionless frequencies versus the variation of different temperature fields of a simply supported FG ZrO_2/Ti−6Al−4V plate is examined. From these figures, it is observed that the frequencies increase with the increase of the ratio b/a when b/a $\leqslant 2$. It is also noted that the frequencies decrease as temperature change increases in all types of temperature fields; this is due to the decrease of the Young's modulus with the increasing of temperature. It is also noted that the decrease of the frequencies in the case where b/a $= 2$ is important compared to the other ratios b/a when the side-to-thickness ratio a/h $= 10$. The uniform temperature fields affect the frequencies more significantly than the linear, nonlinear and sinusoidal temperature fields.

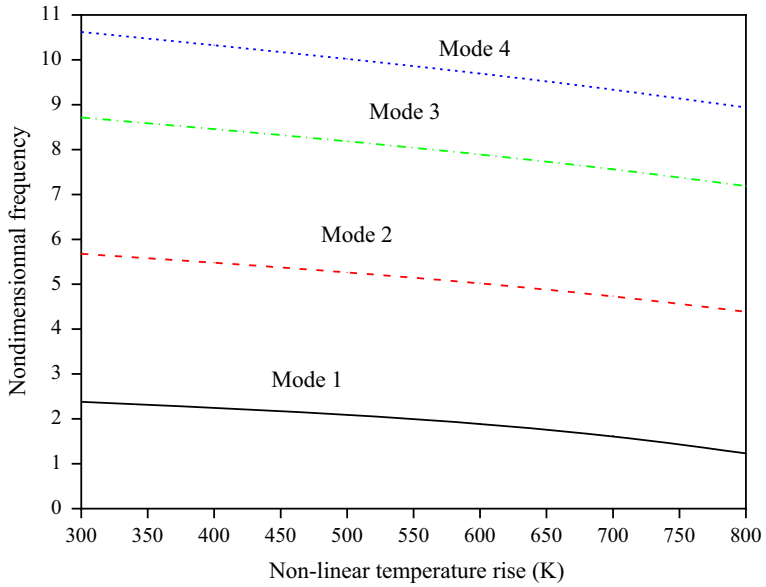

Fig. 9 First four Non-dimensional frequency parameters versus nonlinear temperature field for simply supported ($ZrO_2/Ti-6Al-4V$) FGP when $a/h = 10$, $a = 0.2$, $p = 1$

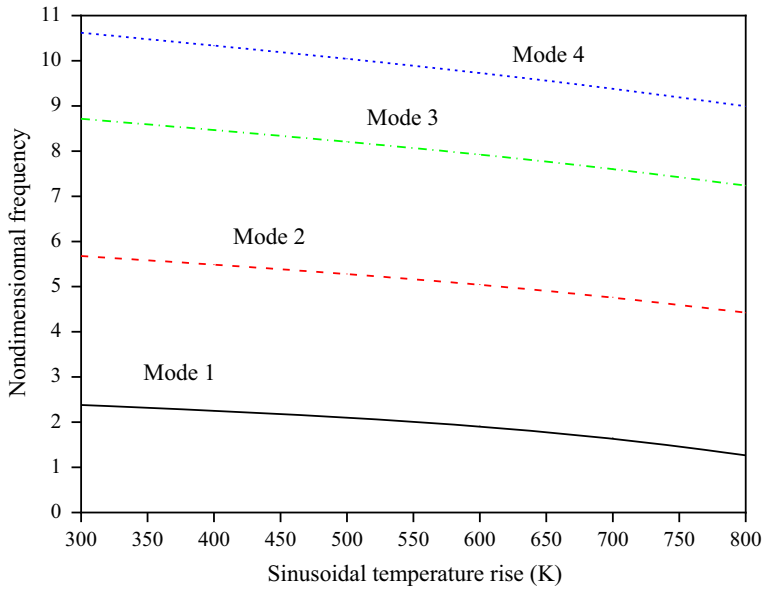

Fig. 10 First four Non-dimensional frequency parameters versus sinusoidal temperature field for simply supported ($ZrO_2/Ti-6Al-4V$) FGP when $a/h = 10$, $a = 0.2$, $p = 1$

Table 6 Non-dimensional natural frequency of temperature dependent (ZrO_2/Ti–6Al–4V) FG plate in thermal environments for different modes of vibration

Mode numbers of FGP (ZrO_2/Ti−6Al−4V) $b = a = 0.2, \quad h = 0.025\ \nu = 0.3$	$T_b = 300(K)$				
	$T_t = 300(K)$	$T_t = 400(K)$		$T_t = 600(K)$	
		Temperature-dependent	Temperature-independent	Temperature-dependent	Temperature-independent
ZrO_2					
(1,1)	8.281	7.810	8.061	6.536	7.604
(1,2)	19.348	18.582	19.116	16.847	18.641
(2,2)	29.225	28.192	28.978	26.009	28. 479
(1,3)	35.301	34.104	34.046	31.640	34.531
$p = 0.5$					
(1,1)	7.118	6.784	6.962	5.933	6.648
(1,2)	16.635	16.097	16.474	14.906	16.148
(2,2)	25.144	24.421	24.974	22.913	24.630
(1,3)	30.383	29.547	30.208	27.844	29.853
$p = 1$					
(1,1)	6.659	6.377	6.531	5.667	6.267
(1,2)	15.562	15.098	15.426	14.087	15.150
(2,2)	23.510	22.888	23.366	21.601	23.076
(1,3)	28.402	27.683	28.253	26.227	27.953
$p = 2$					
(1,1)	6.289	6.049	6.184	5.469	5.968
(1,2)	14.670	14.271	14.558	13.419	14.331
(2,2)	22.133	21.595	22.014	20.499	21.774
(1,3)	26.718	26.096	26.595	24.852	26.346
Ti–6Al–4V					
(1,1)	5.405	5.303	5.362	5.130	5.274
(1,2)	12.628	12.441	12.582	12.093	12.490
(2,2)	19.074	18.812	19.026	18.309	18.927
(1,3)	23.040	22.731	22.989	22.134	22.888

4 Conclusions

A two-dimensional higher-order shear deformation theory has been presented for dynamic analysis of FG plates subjected to uniform, linear, nonlinear and sinusoidal temperature fields. The displacement fields of the presented theory are chosen based on a parabolic distribution of transverse shear strains through the thickness and satisfy the zero traction boundary conditions. The FG plates are assumed to be simply supported with temperature-dependent and independent material properties according to a power law variation. Numerical results are presented for temperature-dependent and temperature-independent FG plate and compared with available results in the literature to check the accuracy of the proposed theory. It can be found that the present theory is efficient and simple in investigating the free vibration response of FG plates exposed to thermal loading. Thus, this work can be used as a reference to assess the validity and establish the accuracy of various approximate theories and to solve the free vibration problems of FG plates under different boundary and environmental conditions.

Table 7 Non-dimensional natural frequency of temperature dependent (Si_3N_4/SUS304) FG plate in thermal environments for different modes of vibration

Mode numbers of FGP (Si_3N_4 et SUS304) $b = a =$ 0.2, $h = 0.025$ $\nu = 0.28$	$T_b = 300(K)$				
	$T_t = 300(K)$	$T_t = 400(K)$		$T_t = 600(K)$	
		Temperature-dependent	Temperature-independent	Temperature-dependent	Temperature-independent
Si_3N_4					
(1,1)	12.507	12.307	12.377	11.887	12.114
(1,2)	29.260	28.964	29.121	28.371	28.843
(2,2)	44.236	43.853	44.090	43.103	43.796
(1,3)	53.460	53.024	53.309	52.176	53.005
(2,3)	66.382	65.310	66.240	64.886	65.906
$p = 0.5$					
(1,1)	8.609	8.453	8.498	8.118	8.272
(1,2)	20.137	19.921	20.020	19.473	19.784
(2,2)	30.441	30.172	30.318	29.621	30.070
(1,3)	36.788	36.485	36.661	35.871	36.405
(2,3)	45.680	45.331	45.547	44.627	45.281
$p = 1$					
(1,1)	7.544	7.399	7.437	7.082	7.217
(1,2)	17.641	17.444	17.528	17.029	17.298
(2,2)	26.661	26.420	26.542	25.913	26.301
(1,3)	32.215	31.946	32.092	31.384	31.970
(2,3)	39.995	39.688	39.867	39.046	39.608
$p = 2$					
(1,1)	6.770	6.631	6.664	6.323	6.447
(1,2)	15.814	15.631	15.702	15.231	15.474
(2,2)	23.879	23.657	23.760	23.173	23.522
(1,3)	28.839	28.594	28.717	28.057	28.471
(2,3)	35.782	35.503	35.654	34.893	35.397
SUS304					
(1,1)	5.410	5.278	5.300	4.945	5.071
(1,2)	12.657	12.495	12.539	12.054	12.301
(2,2)	19.135	18.947	19.012	18.407	18.760
(1,3)	23.126	22.920	22.908	22.320	22.738
(2,3)	28.715	28.487	28.581	27.803	28.310

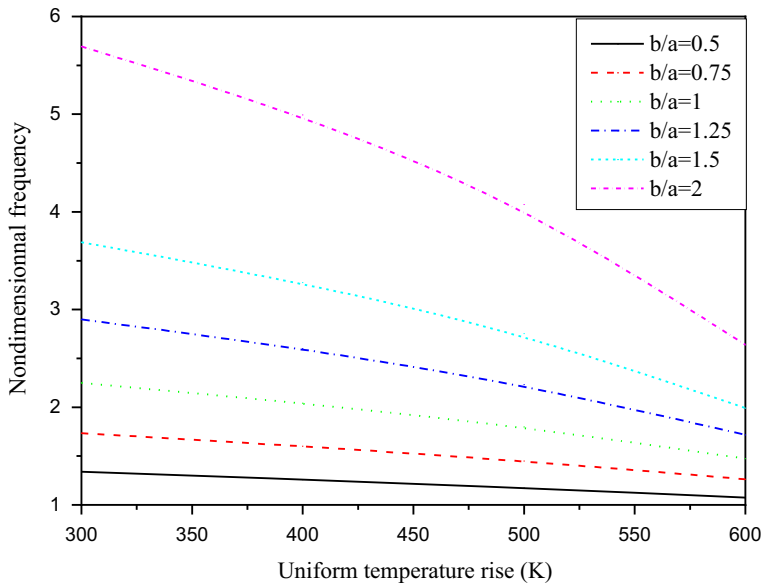

Fig. 11 Non-dimensional frequency parameters versus uniform temperature field for different values of side-to-side ratio (b/a) and simply supported (ZrO_2/Ti−6Al−4V) FGP when $a/h = 10$ and $a = 0.2$, $p = 2$

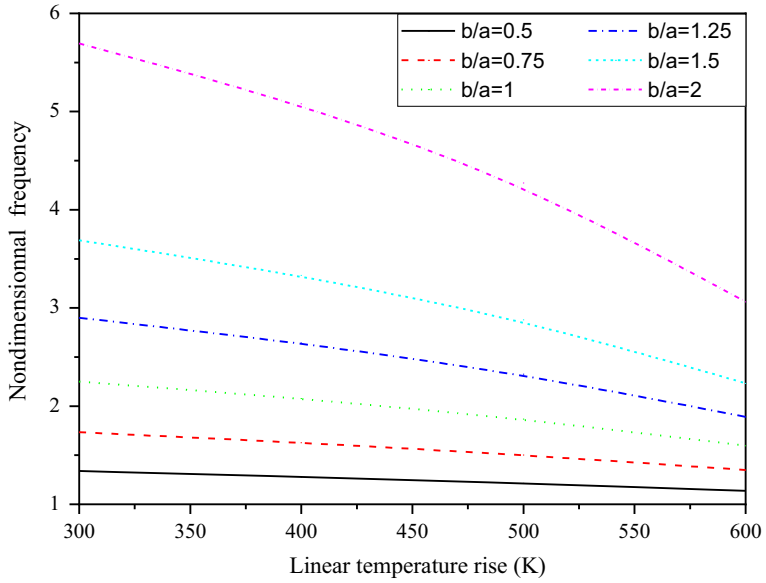

Fig. 12 Non-dimensional frequency parameters versus linear temperature field for different values of side-to-side ratio (b/a) and simply supported (ZrO_2/Ti−6Al−4V) FGP when $a/h = 10$ and $a = 0.2$, $p = 2$

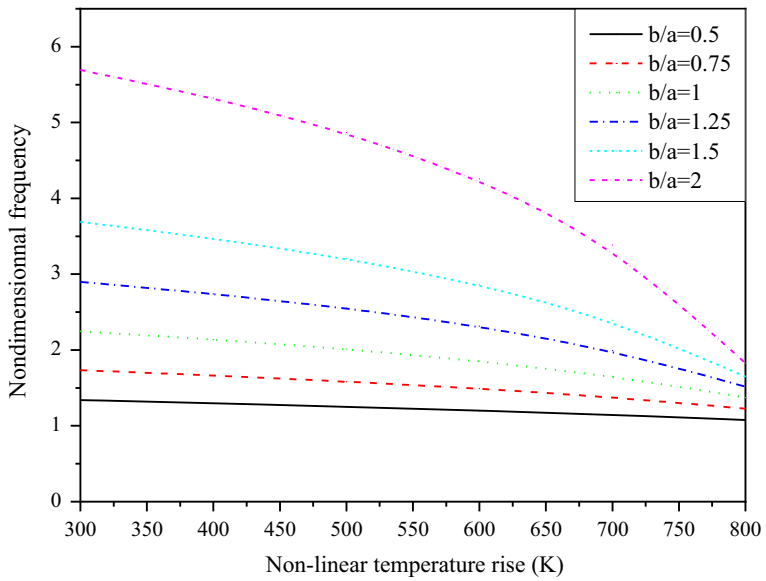

Fig. 13 Non-dimensional frequency parameters versus nonlinear temperature field for different values of side-to-side ratio (b/a) and simply supported (ZrO_2/Ti−6Al−4V) FGP when $a/h = 10$ and $a = 0.2$, $p = 2$

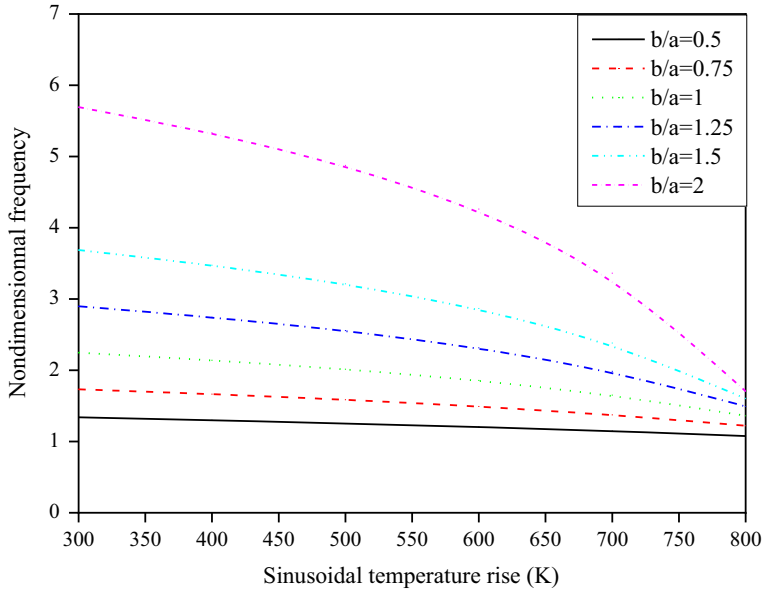

Fig. 14 Non-dimensional frequency parameters versus sinusoidal temperature field for different values of side-to-side ratio (b/a) and simply supported (ZrO_2/Ti−6Al−4V) FGP when $a/h = 10$ and $a = 0.2$, $p = 2$

Acknowledgements The research reported herein was funded by the Deanship of Scientific Research at the University of Hail, Saudi Arabia, through the Project Number RG- 191241. The authors would like to express their deepest gratitude to the Deanship of Scientific Research and to the College of Engineering at the University of Hail for providing necessary support to conducting this research.

References

1. Şimşek, M.: Buckling of Timoshenko beams composed of two-dimensional functionally graded material (2D-FGM) having different boundary conditions. Compos. Struct. **149**, 304–314 (2016). https://doi.org/10.1016/j.compstruct.2016.04.034
2. Ebrahimi, M.J., Najafizadeh, M.M.: Free vibration analysis of two-dimensional functionally graded cylindrical shells. Appl. Math. Model. **38**, 308–324 (2014). https://doi.org/10.1016/j.apm.2013.06.015
3. Lei, Z.X., Zhang, L.W., Liew, K.M.: Buckling analysis of CNT reinforced functionally graded laminated composite plates. Compos. Struct. **152**, 62–73 (2016). https://doi.org/10.1016/j.compstruct.2016.05.047
4. Mehditabar, A., Rahimi, G.H., Vahdat, S.E.: Integrity assessment of functionally graded pipe produced by centrifugal casting subjected to internal pressure: experimental investigation. Arch. Appl. Mech. **90**, 1723–1736 (2020). https://doi.org/10.1007/s00419-020-01692-5
5. Belkhodja, Y., Ouinas, D., Zaoui, F.Z., Fekirini, H.: A higher order exponential-trigonometric shear deformation theory for bending, vibration, and buckling analysis of functionally graded material (FGM) plates: Part I. Advanced Compos Letters **28**, 1–19 (2019). https://doi.org/10.1177/0963693519875739
6. Mantari, J.L., Soares, C.G.: A quasi-3D tangential shear deformation theory with four unknowns for functionally graded plates. Acta Mech. **226**, 625–642 (2015). https://doi.org/10.1007/s00707-014-1192-3
7. Sayyad, A.S., Ghugal, Y.M.: A unified shear deformation theory for the bending of isotropic, functionally graded, laminated and sandwich beams and plates. Int. J. Appl. Mech. **9**, 1750007 (2017)
8. Li, S., Ma, H.: Analysis of free vibration of functionally graded material micro-plates with thermoelastic damping. Arch. Appl. Mech. **90**, 1285–1304 (2020). https://doi.org/10.1007/s00419-020-01664-9
9. Li, Q., Iu, V., Kou, K.: Three-dimensional vibration analysis of functionally graded material plates in thermal environment. J. Sound Vibr. **324**(3–5), 733–750 (2009). https://doi.org/10.1016/j.jsv.2009.02.036
10. Zaoui, F.Z., Tounsi, A., Ouinas, D.: Free vibration of functionally graded plates resting on elastic foundations based on quasi-3D hybrid-type higher order shear deformation theory. Smart Struct. Syst. Int. J. **20**(4), 509–524 (2017). https://doi.org/10.12989/sss.2017.20.4.509
11. Zenkour, A.M., Radwan, A.F.: Hygrothermo-mechanical buckling of FGM plates resting on elastic foundations using a quasi-3D model. Int. J. Comput. Methods Eng. Sci. Mech. **20**(2), 85–98 (2019). https://doi.org/10.1080/15502287.2019.1568618
12. Hieu, P.T., Van Tung, H.: Thermal and thermomechanical buckling of shear deformable FG-CNTRC cylindrical shells and toroidal shell segments with tangentially restrained edges. Arch. Appl. Mech. **90**, 1529–1546 (2020). https://doi.org/10.1007/s00419-020-01682-7
13. Woodward, B., Kashtalyan, M.: Three-dimensional elasticity analysis of sandwich panels with functionally graded transversely isotropic core. Arch. Appl. Mech. **89**, 2463–2484 (2019). https://doi.org/10.1007/s00419-019-01589-y

14. Boroujerdy, M.S., Eslami, M.R.: Nonlinear axisymmetric thermomechanical response of piezo-FGM shallow spherical shells. Arch. Appl. Mech. **83**, 1681–1693 (2013). https://doi.org/10.1007/s00419-013-0769-y
15. Guerroudj, H.Z., Yeghnem, R., Kaci, A., Zaoui, F.Z., Benyoucef, S., Tounsi, A.: Eigenfrequencies of advanced composite plates using an efficient hybrid quasi-3D shear deformation theory. Smart Struct. Syst. Int. J. **22**(1), 121–132 (2018). https://doi.org/10.12989/sss.2018.22.1.121
16. Simsek, M., Cansiz, S.: Dynamics of elastically connected double-functionally graded beam systems with different boundary conditions under action of a moving harmonic load. Compos. Struct. **94**, 2861–2878 (2012). https://doi.org/10.1016/j.compstruct.2012.03.016
17. Amirani, M.C., Khalili, S.M.R., Nemati, N.: Free vibration analysis of sandwich beam with FG core using the element free Galerkin method. Compos. Struct. **90**, 373–379 (2009). https://doi.org/10.1016/j.compstruct.2009.03.023
18. Mahmoudi A, Benyoucef S, Tounsi A, Benachour A, Adda Bedia EA (2018) On the effect of the micromechanical models on the free vibration of rectangular FGM plate resting on elastic foundation.Earthquakes Struct Int J 14(2):117-128.https://doi.org/10.12989/eas.2018.14.2.117
19. Duc, N.D., Tran, Q.Q., Nguyen, D.K.: New approach to investigate nonlinear dynamic response and vibration of imperfect functionally graded carbon nanotube reinforced composite double curved shallow shells subjected to blast load and temperature. Aerosp. Sci. Technol. **71**, 360–372 (2017). https://doi.org/10.1016/j.ast.2017.09.031
20. Shen, H.S.: Nonlinear bending response of functionally graded plates subjected to transverse loads and in thermal environments. Int. J. Mech. Sci. **44**(3), 561–584 (2002). https://doi.org/10.1016/S0020-7403(01)00103-500103-5
21. Yang, J., Shen, H.S.: Vibration characteristics and transient response of shear-deformable functionally graded plates in thermal environments. J. Sound Vibr. **255**(3), 579–602 (2002). https://doi.org/10.1006/jsvi.2001.4161
22. Huang, X., Shen, H.: Nonlinear vibration and dynamic response of functionally graded plates in thermal environments. Int. J. Solids Struct. **41**(9–10), 2403–2427 (2004). https://doi.org/10.1016/j.ijsolstr.2003.11.012
23. Kim, Y.: Temperature dependent vibration analysis of functionally graded rectangular plates. J. Sound Vib. **28**(3–5), 531–549 (2005). https://doi.org/10.1016/j.jsv.2004.06.043
24. Chen, C., Chen, T., Chien, R.: Nonlinear vibration of initially stressed functionally graded plates. Thin-Walled Struct. **44**(8), 844–851 (2006). https://doi.org/10.1016/j.tws.2006.08.007
25. Zenkour, A.M., Alghamdi, N.A.: Thermoelastic bending analysis of functionally graded sandwich plates. J. Mater. Sci. **43**, 2574–89 (2008). https://doi.org/10.1007/s10853-008-2476-6
26. Li, S.R., Su, H.D., Cheng, C.J.: Free vibration of functionally graded material beams with surface-bonded piezoelectric layers in thermal environment. Appl. Math. Mech. **30**(8), 969–982 (2009). https://doi.org/10.1007/s10483-009-0803-7
27. Shariyat, M.: A generalized high-order global-local plate theory for nonlinear bending and buckling analyses of imperfect sandwich plates subjected to thermo-mechanical loads. Compos. Struct. **92**, 130–143 (2010). https://doi.org/10.1016/j.compstruct.2009.07.007
28. Shariyat, M.: A generalized global-local high-order theory for bending and vibration analyses of sandwich plates subjected to thermo-mechanical loads. Int. J. Mech. Sci. **52**, 495–514 (2010). https://doi.org/10.1016/j.ijmecsci.2009.11.010
29. Mahi, A., Adda Bedia, E.A., Tounsi, A., Mechab, I.: An analytical method for temperature dependent free vibration analysis of functionally graded beams with general boundary conditions. Compos. Struct. **92**, 1877–1887 (2010). https://doi.org/10.1016/j.compstruct.2010.01.010
30. Shahrjerdi, A., Mustapha, F., Bayat, M., Majid, D.L.A.: Free vibration analysis of solar functionally graded plates with temperature-dependent material properties using second order shear deformation theory. J. Mech. Sci. Technol. **25**(9), 2195–2209 (2011). https://doi.org/10.1007/s12206-011-0610-x
31. Kiani, Y., Eslami, M.R.: Thermal buckling and post-buckling response of imperfect temperature-dependent sandwich FGM plates resting on elastic foundation. Arch. Appl. Mech. **82**(7), 891–905 (2012). https://doi.org/10.1007/s00419-011-0599-8
32. Malekzadeh, P., Monajjemzadeh, S.M.: Dynamic response of functionally graded plates in thermal environment under moving load. J. Compos. B **45**, 1521–1533 (2013). https://doi.org/10.1016/j.compositesb.2012.09.022
33. Zhang, D.: Nonlinear bending analysis of FGM rectangular plates with various supported boundaries resting on two-parameter elastic foundations. Arch. Appl. Mech. **84**, 1–20 (2014). https://doi.org/10.1007/s00419-013-0775-0
34. Nejati, M., Fard, K.M., Eslampanah, A.: Effects of fiber orientation and temperature on natural frequencies of a functionally graded beam reinforced with fiber. J. Mech. Sci. Technol. **29**, 3363–3371 (2015). https://doi.org/10.1007/s12206-015-0734-5
35. Fazzolari, F.A.: Natural frequencies and critical temperatures of functionally graded sandwich plates subjected to uniform and non-uniform temperature distributions. Compos. Struct. **121**, 197–210 (2015). https://doi.org/10.1016/j.compstruct.2014.10.039
36. Kar, V.R., Panda, S.K.: Free vibration responses of temperature dependent functionally graded curved panels under thermal environment. Latin Am. J. Solids Struct. **12**(11), 2006–2024 (2015). https://doi.org/10.1590/1679-78251691
37. Attia, A., Tounsi, A., Adda Bedia, E.A., Mahmoud, S.R.: Free vibration analysis of functionally graded plates with temperature-dependent properties using various four variable refined plate theories. Steel Compos. Struct. **18**(1), 187–212 (2015). https://doi.org/10.12989/scs.2015.18.1.187
38. Ibrahimi, F., Barati, M.R.: Temperature distribution effects on buckling behavior of smart heterogeneous nanosize plates based on nonlocal four-variable refined plate theory. Int. J. Smart Nano Mater. **7**(3), 119–143 (2016). https://doi.org/10.1080/19475411.2016.1223203
39. Wang, Y.Q., Zu, J.W.: Vibration behaviors of functionally graded rectangular plates with porosities and moving in thermal environment. Aerosp. Sci. Technol. **69**, 550–562 (2017). https://doi.org/10.1016/j.ast.2017.07.023
40. Taleb, O., Houari, M.S.A., Bessaim, A., Tounsi, A., Mahmoud, S.R.: A new plate model for vibration response of advanced composite plates in thermal environment. Struct. Eng. Mech. Int. J. **67**(4), 369–383 (2018). https://doi.org/10.12989/sem.2018.67.4.369
41. Shahsavari, D., Shahsavari, M., Li, L., Karami, B.: A novel quasi-3D hyperbolic theory for free vibration of FG plates with porosities resting on Winkler/Pasternak/Kerr foundation. Aerosp. Sci. Technol. **72**, 134–149 (2018). https://doi.org/10.1016/j.ast.2017.11.004

42. Thang, P.T., Nguyen-Thoi, T., Lee, D., Kang, J., Lee, J.: Elastic buckling and free vibration analyses of porous-cellular plates with uniform and non-uniform porosity distributions. Aerosp. Sci. Technol. **79**, 278–287 (2018). https://doi.org/10.1016/j.ast.2018.06.010
43. Tu, T.M., Quoc, T.H., Van Long, N.: Vibration analysis of functionally graded plates using the eight-unknown higher order shear deformation theory in thermal environments. Aerosp. Sci. Technol. **84**, 698–711 (2019). https://doi.org/10.1016/j.ast.2018.11.010
44. Zaoui, F.Z., Ouinas, D., Tounsi, A.: New 2D and quasi-3D shear deformation theories for free vibration of functionally graded plates on elastic foundations. Compos. Part B Eng. **159**, 231–247 (2019). https://doi.org/10.1016/j.compositesb.2018.09.051
45. Azadi, M.: Free and forced vibration analysis of FG beam considering temperature dependency of material properties. J. Mech. Sci. Technol. **25**(1), 69–80 (2011). https://doi.org/10.1007/s12206-010-1015-y
46. Touloukian, Y.S.: Thermophysical Properties of High Temperature Solid Materials. MacMillan, New York (1967)
47. Reddy, J.N., Chin, C.D.: Thermo-mechanical analysis of functionally graded cylinders and plates. J. Therm. Stress. **21**, 593–626 (1998). https://doi.org/10.1080/01495739808956165
48. Javaheri, R., Eslami, M.: Thermal buckling of functionally graded plates based on higher order theory. J. Therm. Stress. **25**(7), 603–625 (2002). https://doi.org/10.1080/01495730290074333
49. Mokhtar, B., Abedlouahed, T., Adda Bedia, E.A., Abdelkader, M.: Buckling analysis of functionally graded plates with simply supported edges. Leonardo J. Sci. **8**, 21–32 (2009)
50. Esmaeilzadeh, M., Kadkhodayan, M.: Dynamic analysis of stiffened bi-directional functionally graded plates with porosities under a moving load by dynamic relaxation method with kinetic damping. Aerosp. Sci. Technol. **93**, 105333 (2019). https://doi.org/10.1016/j.ast.2019.105333
51. Li, Q., Iu, V., Kou, K.: Three-dimensional vibration analysis of functionally graded material plates in thermal environment. J. Sound Vib. **324**(3–5), 733–750 (2009). https://doi.org/10.1016/j.jsv.2009.02.036